

# Focusing Spaceborne/Airborne Hybrid Bistatic SAR Data Using Wavenumber-Domain Algorithm

Robert Wang, *Member, IEEE*, Otmar Loffeld, *Senior Member, IEEE*,  
Holger Nies, and Joachim H. G. Ender, *Senior Member, IEEE*

**Abstract**—This paper focuses on the bistatic synthetic aperture radar (SAR) data processing in a spaceborne/airborne hybrid bistatic configuration. Due to the extreme differences in platform velocities and slant ranges, the airborne system operates in the inverse sliding-spotlight mode, while the spaceborne system works in the sliding-spotlight mode to achieve a tradeoff between azimuth scene size and azimuth resolution. In this extreme bistatic configuration, our original bistatic formula shows a limitation of accurately describing the bistatic point-target reference spectrum, owing to the assumption of equal contributions of transmitter and receiver to the total Doppler spectrum. We extend our previous formula using the weighting operation where the weighting factor is the ratio of the azimuth time-bandwidth product (TBP) of the platform to the total azimuth TBP. In this paper, the bistatic-deformation and azimuth-dependent range-cell-migration terms were removed with phase multiplications performed blockwise in range-azimuth subsections. The remaining quasi-monostatic term shows the characteristic of the conventional monostatic SAR besides an additional azimuth-scaling term. For the monostatic characteristic, any precision monostatic SAR processing algorithms can handle. In this paper, we prefer the wavenumber-domain algorithm (also known as Omega-K), since it can accurately correct the range dependence of the range-azimuth coupling, as well as the azimuth-frequency dependence. For the azimuth-scaling term, an inverse scaled Fourier transformation is performed to correct it. Finally, a hybrid spaceborne/airborne simulation experiment is conducted to validate the proposed processing procedure.

**Index Terms**—Bistatic point-target reference spectrum (BPTRS), bistatic synthetic aperture radar (BiSAR), range cell migration (RCM), time-bandwidth product (TBP).

## NOMENCLATURE

$\tau, t$	Azimuth and range time variables.
$\tau_{0R}, \tau_{0T}$	Zero Doppler times of receiver and transmitter, respectively.
$R_{0R}, R_{0T}$	Closest ranges from receiver and transmitter to the point target $P(\tau_{0R}, R_{0R})$ , respectively.
$(\tau_{0R}, R_{0R})$	Receiver-referenced coordinates defined as the coordinates of image space.

Manuscript received April 14, 2008; revised July 30, 2008 and October 20, 2008. First published April 7, 2009; current version published June 19, 2009. This work was supported by the Germany Science Foundation under Grant Lo 455/7-1 BiFocus.

R. Wang, O. Loffeld, and H. Nies are with the Center for Sensorsystems, University of Siegen, 57076 Siegen, Germany (e-mail: wang@zess.uni-siegen.de).

J. H. G. Ender is with the Research Institute for High Frequency Physics and Radar Techniques, Forschungsgesellschaft für Angewandte Naturwissenschaften, 53343 Wachtberg, Germany.

Color versions of one or more of the figures in this paper are available online at <http://ieeexplore.ieee.org>.

Digital Object Identifier 10.1109/TGRS.2008.2010852

$\sigma(\tau_{0R}, R_{0R})$	Backscattering coefficient of the point target located at $(\tau_{0R}, R_{0R})$ .
$R_m$	Closest range from the scene center to the ideal trajectory of receiver.
$r$	Zero-offset receiver-to-target range variable defined by $r = R_{0R} - R_m$ .
$v_R, v_T$	Platform velocities of receiver and transmitter, respectively.
$c$	Speed of light.
$\lambda, f_0$	Carrier wavelength and carrier frequency of the transmitted signal, respectively.
$f, f_\tau$	Range and azimuth-frequency variables.

## I. INTRODUCTION

**B**ISTATIC synthetic aperture radar (BiSAR) is characterized by different locations for transmitter and receiver and, hence, offers considerable flexibility in designing BiSAR missions [1], [2]. However, this flexibility configuration is paid by a huge processing complication, since the bistatic range equation consists of a double square-root term. Therefore, the bistatic point-target reference spectrum (BPTRS) does not offer the analytical simplicity of the single square root in monostatic SAR using the principle of stationary phase (PSP), which implies that monostatic processing algorithms cannot be directly applied [3]–[14].

In [4], based on an approximately analytical BPTRS, the 2-D inverse-scaled Fourier transform (ISFT) is applied to focus BiSAR data. Using the numerical solutions of the double square-root phase term, wavenumber-domain algorithm is also used to focus BiSAR data [7] where only azimuth-invariant configurations are handled. In addition, a numerical transfer function for BiSAR has been published in [8], where a standard SAR processor can be used to process the BiSAR data of azimuth-invariant configurations. In [9], a preprocessing technique known as dip move out is employed to transform the azimuth-invariant bistatic configuration to the monostatic one. A modified range-Doppler algorithm is proposed to process space-surface BiSAR data in [10], where it is suitable for stripmap space-surface bistatic configuration. In particular, based on an analytical BPTRS [11], a nonlinear chirp-scaling algorithm and range-Doppler algorithm has been used to process BiSAR data [12], [13].

Loffeld's bistatic formula (LBF) has been originally developed for the general bistatic configuration in [2] with the assumption of the equal contributions of both range equations to the total Doppler spectrum. This assumption is no longer valid in the hybrid spaceborne/airborne case where transmitter and

receiver highly differ in the velocities and slant ranges [14]. The considerable differences in velocity and slant range result in unequal contributions of both range equations to the total Doppler spectrum [14]. In order to focus the spaceborne/airborne hybrid configuration, we have developed the extended LBF (ELBF) in [5], where the time-bandwidth products (TBPs) of the phase histories of transmitter and receiver are used to weigh the contributions of transmitter and receiver to the total Doppler spectrum. Aiming at the planned spaceborne/airborne experiment (TerraSAR-X as the illuminator and the airborne SAR system PAMIR of FGAN as the bistatic receiver [15], [16]), the accuracy of ELBF has been validated in [14].

The ELBF still consists of two components: quasi-monostatic (QM) phase term and bistatic-deformation (BD) phase term. In this paper, we first linearize the QM term, factor out the azimuth-dependent range-cell-migration (RCM) component, and incorporate it into the BD term. Then, we remove the new BD term using phase multiplication in range-azimuth subsections [4]. Subsequently, for the convenience of processing, the remaining QM term is decomposed into three components: range-invariant, range-variant, and azimuth-scaling terms. The range-invariant and range-variant terms are the inherent components of the conventional monostatic SAR [6]. Therefore, after compensating the new BD term, only an additional azimuth-scaling term is left in the remaining QM term as compared with the monostatic spectrum [6]. Thus, the well-known monostatic SAR algorithms (e.g., range-Doppler, chirp-scaling, and Omega-K algorithms) can be applied to focus the BiSAR data. In this paper, the range-invariant term is removed with reference phase multiplication; for the range-variant term, we adopt the Stolt interpolation to correct its nonlinear dependence on the range and azimuth frequencies [6], [17]. Finally, the azimuth-scaling term can be corrected with ISFT or interpolation.

This paper is organized as follows. In Section II, the ELBF is derived and explained. Moreover, the further overview of our weighting idea is left to the Appendix. Section III describes the processing procedure with the wavenumber-domain algorithm (WDA). Some simulations to verify the proposed processing method are performed in Section IV. Finally, some conclusions are reported in Section V.

## II. ELBF

In this paper, we consider the bistatic geometry in the hybrid spaceborne/airborne configuration, as shown in Fig. 1. The mathematical symbols and their definitions used in this paper are given in the Nomenclature. The received signal from a point target located at  $(\tau_{0R}, R_{0R})$  after demodulation is given by

$$g(\tau, t, \tau_{0R}, R_{0R}) = \sigma(\tau_{0R}, R_{0R}) s_l \left( t - \frac{R_R(\tau) + R_T(\tau)}{c} \right) \times \exp \left[ -j2\pi \frac{R_R(\tau) + R_T(\tau)}{\lambda} \right] w(\tau - \tau_{cb}) \quad (1)$$

where  $w(\tau - \tau_{cb})$  is the composite azimuth antenna pattern centered on azimuth time  $\tau_{cb}$ .  $s_l(t)$  represents the transmitted signal.  $R_R(\tau)$  and  $R_T(\tau)$  are the instantaneous slant ranges

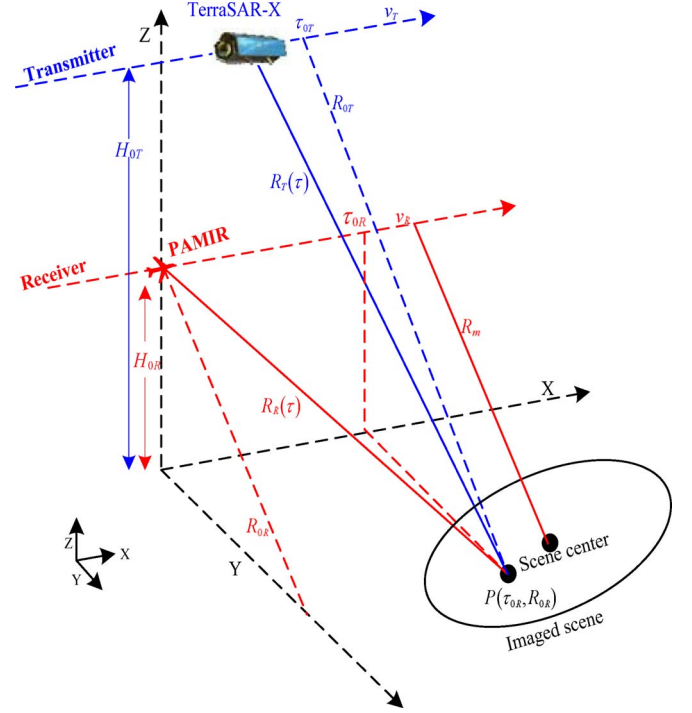


Fig. 1. Imaging geometry of the spaceborne/airborne BiSAR configuration.  $X$ ,  $Y$ , and  $Z$  represent the along-track, cross-track, and vertical directions, respectively.

from receiver and transmitter, respectively, to the point target, defined as

$$R_R(\tau) = \sqrt{R_{0R}^2 + (\tau - \tau_{0R})^2 v_R^2} \\ R_T(\tau) = \sqrt{R_{0T}^2 + (\tau - \tau_{0T})^2 v_T^2}. \quad (2)$$

Performing the Fourier transformation (FT) with respect to the range time variable  $t$ , we can transform (1) into the range-frequency/azimuth-time domain

$$G(\tau, f, \tau_{0R}, R_{0R}) = \sigma(\tau_{0R}, R_{0R}) S_1(f) w(\tau - \tau_{cb}) \times \exp \left[ -2\pi(f + f_0) \frac{R_R(\tau) + R_T(\tau)}{c} \right] \quad (3)$$

where  $S_1(f)$  is the baseband spectrum of the transmitted signal.

Then, an azimuth FT is performed to transform the signal into the 2-D frequency domain.

$$G(f_\tau, f, \tau_{0R}, R_{0R}) = \sigma(\tau_{0R}, R_{0R}) S_1(f) \times \int w(\tau - \tau_{cb}) \exp[-j\phi_b(\tau, f_\tau)] d\tau \quad (4)$$

where

$$\phi_b(\tau, f) = 2\pi(f + f_0) \frac{R_R(\tau) + R_T(\tau)}{c} + 2\pi f_\tau \tau. \quad (5)$$

Because of the double square root contained in the integral of (4), the PSP cannot directly be applied to obtain the bistatic

stationary point. To circumvent this limitation, two equivalent terms are introduced into (5) [2]

$$\phi_b(\tau, f) = \phi_R(\tau) + \phi_T(\tau) \quad (6)$$

where

$$\begin{aligned} \phi_R(\tau) &= 2\pi \left[ \frac{f + f_0}{c} R_R(\tau) + \frac{f_\tau \tau}{2} \right] \\ \phi_T(\tau) &= 2\pi \left[ \frac{f + f_0}{c} R_T(\tau) + \frac{f_\tau \tau}{2} \right]. \end{aligned} \quad (7)$$

From (7), it can be seen that we equalize the contributions of both range equations to the total Doppler frequency. In the spaceborne/airborne hybrid configuration, the contributions are considerably different due to the extreme difference in slant range and velocity of transmitter and receiver, which results in the degradation of the LBF.

In this paper, we adopt the TBP to weigh contributions of the range equations of transmitter and receiver to the instantaneous Doppler frequency. This weighting operation will result in the fact that the azimuth modulations of both range equations will well agree with the individual instantaneous Doppler frequencies (see Appendix). Therefore, (6) can be reformulated as

$$\begin{aligned} \phi_b(\tau, f) &= 2\pi \left\{ \frac{f + f_0}{c} [R_R(\tau) + R_T(\tau)] + (k_R + k_T) f_\tau \tau \right\} \\ &= \phi_{RW}(\tau, f) + \phi_{TW}(\tau, f) \end{aligned} \quad (8)$$

where

$$\begin{aligned} \phi_{RW}(\tau, f) &= 2\pi \left[ \frac{f + f_0}{c} R_R(\tau) + k_R f_\tau \tau \right] \\ \phi_{TW}(\tau, f) &= 2\pi \left[ \frac{f + f_0}{c} R_T(\tau) + k_T f_\tau \tau \right] \\ k_T &= \frac{TBP_T}{TBP_R + TBP_T} \\ &= \frac{(v_T^2 / \lambda R_{0T}) T_a^2}{(v_R^2 / \lambda R_{0R}) T_a^2 + (v_T^2 / \lambda R_{0T}) T_a^2} \\ k_R &= \frac{TBP_R}{TBP_R + TBP_T} \\ &= \frac{(v_R^2 / \lambda R_{0R}) T_a^2}{(v_R^2 / \lambda R_{0R}) T_a^2 + (v_T^2 / \lambda R_{0T}) T_a^2}. \end{aligned} \quad (9)$$

$TBP_R$  and  $TBP_T$  are the TBPs of the azimuth-modulation signals from receiver and transmitter, respectively. For the calculation of TBPs, we use the composite synthetic aperture time  $T_a$ . Therefore, the weighting factor based on the TBPs is also equivalent to using the azimuth chirp rates and Doppler bandwidths. The reason for using the TBP as the weighting factor is that it can be seen as indicators of modulation degree of a chirp signal [6]. From (10), it is clear that we always have  $k_R + k_T = 1$ . Via this weighting operation, the contributions of receiver and transmitter to the azimuth Doppler spectrum are restricted by the factors  $k_R$  and  $k_T$ , respectively. Equation (7) is only the special case of (9) when contributions of transmitter and receiver are equally weighted ( $k_R = k_T = 1/2$ ).

To address the problem of double square-root term, we expand  $\phi_{RW}$  and  $\phi_{TW}$  in second-order Taylor series around their stationary points:  $\tilde{\tau}_{RW}$  and  $\tilde{\tau}_{TW}$  [2]. These two quadratic functions are given as

$$\begin{aligned} \phi_{RW}(\tau, f) &\approx \phi_{RW}(\tilde{\tau}_{RW}, f) + \frac{1}{2} \ddot{\phi}_{RW}(\tilde{\tau}_{RW}, f) (\tau - \tilde{\tau}_{RW})^2 \\ \phi_{TW}(\tau, f) &\approx \phi_{TW}(\tilde{\tau}_{TW}, f) + \frac{1}{2} \ddot{\phi}_{TW}(\tilde{\tau}_{TW}, f) (\tau - \tilde{\tau}_{TW})^2 \end{aligned} \quad (11)$$

where  $\tilde{\tau}_{WR}$  and  $\tilde{\tau}_{WT}$  are defined as

$$\begin{aligned} \tilde{\tau}_{RW} &= \tau_{0R} - k_R \frac{c R_{0R}}{v_R^2} \frac{f_\tau}{F_{RW}} \\ \tilde{\tau}_{TW} &= \tau_{0T} - k_T \frac{c R_{0T}}{v_T^2} \frac{f_\tau}{F_{TW}} \end{aligned} \quad (12a)$$

$$\begin{aligned} F_{RW} &= \sqrt{(f + f_0)^2 - \left( \frac{k_R c f_\tau}{v_R} \right)^2} \\ F_{TW} &= \sqrt{(f + f_0)^2 - \left( \frac{k_T c f_\tau}{v_T} \right)^2}. \end{aligned} \quad (12b)$$

To obtain the bistatic stationary point, substituting (11) into (8) yields

$$\begin{aligned} \phi_b(\tau, f) &\approx \phi_{RW}(\tilde{\tau}_{RW}, f) + \frac{1}{2} \ddot{\phi}_{RW}(\tilde{\tau}_{RW}, f) (\tau - \tilde{\tau}_{RW})^2 \\ &\quad + \phi_{TW}(\tilde{\tau}_{TW}, f) + \frac{1}{2} \ddot{\phi}_{TW}(\tilde{\tau}_{TW}, f) (\tau - \tilde{\tau}_{TW})^2. \end{aligned} \quad (13)$$

Applying the PSP to (13) yields the common stationary point as

$$\left. \frac{d\phi_b(\tau, f)}{d\tau} \right|_{\tau=\tilde{\tau}_W} = 0. \quad (14)$$

Solving (14) for  $\tilde{\tau}_W$  yields

$$\begin{aligned} \tilde{\tau}_W &= \frac{\ddot{\phi}_{RW}(\tilde{\tau}_{RW}, f) \times \tilde{\tau}_{RW} + \ddot{\phi}_{TW}(\tilde{\tau}_{TW}, f) \times \tilde{\tau}_{TW}}{\ddot{\phi}_{RW}(\tilde{\tau}_{RW}, f) + \ddot{\phi}_{TW}(\tilde{\tau}_{TW}, f)} \\ &= \frac{R_{0T} v_R^2 F_{RW}^3 \tau_{0R} + R_{0R} v_T^2 F_{TW}^3 \tau_{0T}}{R_{0T} v_R^2 F_{RW}^3 + R_{0R} v_T^2 F_{TW}^3} \\ &\quad - c f_\tau \frac{R_{0R} R_{0T} (k_R F_{RW}^2 + k_T F_{TW}^2)}{R_{0T} v_R^2 F_{RW}^3 + R_{0R} v_T^2 F_{TW}^3}. \end{aligned} \quad (15)$$

Evaluation of (4) proceeds by substituting  $\tilde{\tau}_W$  for  $\tau$  in the right-hand side of (4) and disregarding the nonessential complex factor. The result is

$$\begin{aligned} G(f_\tau, f, \tau_{0R}, R_{0R}) &= \sigma(\tau_{0R}, R_{0R}) S_1(f) w(\tilde{\tau}_W - \tau_{cb}) \\ &\quad \times \exp[-j\Psi_{QMW}(f_\tau, f, R_{0R})] \exp\left[-j\frac{\Psi_{BDW}(f_\tau, f, R_{0R})}{2}\right] \end{aligned} \quad (16)$$

where  $\Psi_{\text{QMW}}$  and  $\Psi_{\text{BDW}}$  refer to the QM and BD terms, respectively. They are defined as

$$\begin{aligned}\Psi_{\text{QMW}}(f_\tau, f, R_{0R}) &= \phi_{WR}(\tilde{\tau}_{WR}, f) + \phi_{WT}(\tilde{\tau}_{WT}, f) \\ &= 2\pi f_\tau(k_R\tau_{0T} + k_T\tau_{0R}) + \frac{2\pi}{c}(R_{0R}F_{RW} + R_{0T}F_{TW})\end{aligned}\quad (17)$$

$$\begin{aligned}\Psi_{\text{BDW}}(f_\tau, f, R_{0R}) &= \ddot{\phi}_{RW}(\tilde{\tau}_{RW}, f)(\tilde{\tau}_W - \tilde{\tau}_{RW})^2 \\ &\quad + \ddot{\phi}_{TW}(\tilde{\tau}_{TW}, f)(\tilde{\tau}_W - \tilde{\tau}_{TW})^2 \\ &= \frac{2\pi v_R^2 v_T^2 F_{RW}^3 F_{TW}^3}{c(f + f_0)^2 (R_{0R}v_T^2 F_{TW}^3 + R_{0T}v_R^2 F_{RW}^3)} \\ &\quad \times \left[ (\tau_{0T} - \tau_{0R}) - \frac{cf_\tau}{v_R^2 v_T^2 F_{RW} F_{TW}} \right. \\ &\quad \left. \times (k_T R_{0T} v_R^2 F_{RW} - k_R R_{0R} v_T^2 F_{TW}) \right]^2.\end{aligned}\quad (18)$$

In [2], the QM and BD terms are defined as

$$\begin{aligned}\Psi_{\text{QM}}(f_\tau, f, R_{0R}) &= 2\pi f_\tau(\tau_{0T} + \tau_{0R}) + \frac{2\pi}{c}(R_{0R}F_R + R_{0T}F_T)\end{aligned}\quad (17a)$$

$$\begin{aligned}\Psi_{\text{BD}}(f_\tau, f, R_{0R}) &= \frac{2\pi v_R^2 v_T^2 F_R^3 F_T^3}{c(f + f_0)^2 (R_{0R}v_T^2 F_T^3 + R_{0T}v_R^2 F_R^3)} \\ &\quad \times \left[ (\tau_{0T} - \tau_{0R}) - \frac{cf_\tau}{2v_R^2 v_T^2 F_R F_T} \right. \\ &\quad \left. \times (R_{0T}v_R^2 F_R - R_{0R}v_T^2 F_T) \right]^2\end{aligned}\quad (18a)$$

where

$$\begin{aligned}F_R &= \sqrt{(f + f_0)^2 - \left(\frac{cf_\tau}{2v_R}\right)^2} \\ F_T &= \sqrt{(f + f_0)^2 - \left(\frac{cf_\tau}{2v_T}\right)^2}.\end{aligned}\quad (19)$$

Comparing (17) and (18) and (17a) and (18a), it can be seen that  $\Psi_{\text{QMW}}$  and  $\Psi_{\text{BDW}}$  would be equal to  $\Psi_{\text{QM}}$  and  $\Psi_{\text{BD}}$  if letting  $k_R = k_T = 1/2$ .

### III. WDA FOR THE SPACEBORNE/AIRBORNE HYBRID BiSAR DATA

In this section, we begin with the 2-D linearization of  $\Psi_{\text{QMW}}$ . We bilinearly express  $\tau_{0T}$ ,  $R_{0T}$ , and  $R_{0R}$  in terms of  $(\tau_{0R}, r)$  [4].

$$\begin{aligned}\tau_{0T} &= p_{10} + p_{11}r + p_{12}\tau_{0R} \\ R_{0T} &= p_{20} + p_{21}r + p_{22}\tau_{0R} \\ R_{0R} &= r + R_m.\end{aligned}\quad (20)$$

Substituting (20) into (17) yields

$$\begin{aligned}\Psi_{\text{QMW}}(f_\tau, f, r) &\approx 2\pi p_{10}k_T f_\tau + 2\pi p_{11}rk_T f_\tau \\ &\quad + 2\pi(k_T p_{12} + k_R)\tau_{0R}f_\tau + \frac{2\pi}{c}p_{22}\tau_{0R}F_{TW} \\ &\quad + \frac{2\pi}{c}(r + R_m)F_{RW} + \frac{2\pi}{c}(p_{20} + p_{21}r)F_{TW}.\end{aligned}\quad (21)$$

From (21), it can be seen that  $2\pi p_{22}\tau_{0R}F_{TW}/c$  contains an azimuth-dependent RCM term which is introduced by the azimuth-variant baseline between transmitter and receiver. For clarity, we expand  $F_{TW}$  with respect to  $f_\tau$  and  $f$  as

$$\begin{aligned}\frac{2\pi}{c}p_{22}\tau_{0R}F_{TW} &\approx \left[ \sqrt{f_0^2 - \left(\frac{k_T c f_{Dc}}{v_T}\right)^2} + \frac{\left(\frac{k_T c f_{Dc}}{v_T}\right)^2}{\sqrt{f_0^2 - \left(\frac{k_T c f_{Dc}}{v_T}\right)^2}} \right. \\ &\quad \left. + \frac{f}{\sqrt{1 - \left(\frac{k_T \lambda f_{Dc}}{v_T}\right)^2}} - \frac{\left(\frac{k_T c}{v_T}\right)^2 f_{Dc}}{\sqrt{f_0^2 - \left(\frac{k_T c f_{Dc}}{v_T}\right)^2}} \right] f_\tau \frac{2\pi p_{22}\tau_{0R}}{c}\end{aligned}\quad (22)$$

where  $f_{Dc}$  specifies the Doppler centroid of azimuth signal. In (22), the first two terms represent the residual phase terms and are negligible if a magnitude image is the final product; the third term is the azimuth-dependent RCM; the last term denotes the azimuth-scaling term [4].

This azimuth-dependent RCM term must be removed after azimuth compression and registration. However, this leads to a conflict: It is known that the focusing quality of azimuth compression will be affected by the accuracy of the RCM correction. To deal with the conflict, we will factor out the azimuth-dependent RCM from (21) and incorporate it into  $\Psi_{\text{BDW}}$ . The new expressions of QM and BD are then given as

$$\begin{aligned}\bar{\Psi}_{\text{QMW}}(f_\tau, f, r) &= 2\pi p_{10}k_T f_\tau + 2\pi p_{11}rk_T f_\tau + \frac{2\pi}{c}(r + R_m)F_{RW} \\ &\quad + \frac{2\pi}{c}(p_{20} + p_{21}r)F_{TW} + 2\pi\beta_A\tau_{0R}f_\tau\end{aligned}\quad (23)$$

$$\begin{aligned}\bar{\Psi}_{\text{BDW}}(f_\tau, f, R_{0R}) &= \Psi_{\text{BD}}(f_\tau, f) + \frac{4\pi p_{22}\tau_{0R}f}{c\sqrt{1 - \left(\frac{k_T \lambda f_{Dc}}{v_T}\right)^2}}\end{aligned}\quad (24)$$

where the nonessential phase terms [i.e., the first two terms in (22)] have been neglected, the azimuth-scaling factor  $\beta_A$  is defined as

$$\beta_A = k_T p_{12} + k_R - \frac{p_{22}\lambda k_T^2 f_{Dc}}{v_T^2 \sqrt{1 - \left(\frac{k_T \lambda f_{Dc}}{v_T}\right)^2}}.\quad (25)$$

Some short remarks concerning (23) and (24) will be helpful to understand the idea.

- 1)  $\bar{\Psi}_{\text{BDW}}(f_\tau, f, R_{0R})$  includes the 2-D space-variant RCM, range-azimuth coupling, azimuth scaling, and azimuth modulation. To deal with  $\bar{\Psi}_{\text{BDW}}$ , we perform a

preprocessing operation in the range–azimuth subsections to remove it [4]. For each subsection, the correction factor for  $\bar{\Psi}_{BDW}$  is substituted by averaged values over slant range and azimuth time.

- 2) After removing  $\bar{\Psi}_{BDW}$ ,  $\bar{\Psi}_{QMW}$  shows an additional azimuth-scaling term as compared with the conventional monostatic spectrum [6]. Therefore, any efficient monostatic processing algorithms can be applied to focus the BiSAR data.

After preprocessing, (16) becomes

$$\bar{G}(f_\tau, f, \tau_{0R}, r) = \sigma(\tau_{0R}, R_{0R}) S_1(f) w(\tilde{\tau}_W - \tau_{cb}) \times \exp[-j\bar{\Psi}_{QMW}(f_\tau, f, r)]. \quad (26)$$

For further clarity, we decompose  $\bar{\Psi}_{QMW}$  into a range-invariant, range-variant, and azimuth-scaling terms

$$\bar{\Psi}_{QMW}(f_\tau, f, r) = \underbrace{\Phi_{IV}(f_\tau, f) + \Phi_V(f_\tau, f, r)}_{\text{Monostatic}} + \Phi_{AS}(f_\tau) \quad (27)$$

where the range-invariant, range-variant, and azimuth-scaling terms are denoted by the subscripts <sub>IV</sub>, <sub>V</sub> and <sub>AS</sub>

$$\Phi_{IV}(f_\tau, f) = 2\pi k_T p_{10} f_\tau + \frac{2\pi}{c} R_m F_{RW} + \frac{2\pi}{c} p_{20} F_{TW} \quad (28)$$

$$\Phi_V(f_\tau, f, r) = 2\pi \frac{(1 + p_{21})r}{c} \frac{[cp_{11}k_T f_\tau + (F_{RW} + p_{21}F_{TW})]}{(1 + p_{21})} \quad (29)$$

$$\Phi_{AS}(f_\tau) = 2\pi \beta_A \tau_{0R} f_\tau. \quad (30)$$

For clarity, some further comments concerning (28)–(30) are given as follows.

- 1)  $\Phi_{IV}(f_\tau, f)$  represents the range-invariant component. It is responsible for the range-invariant RCM, range–azimuth coupling, and azimuth modulation. It can be removed with reference function multiplication (RFM) in the 2-D frequency domain [6].
- 2)  $\Phi_V(f_\tau, f, r)$  is the range-variant component. It accounts for the range-variant RCM, range–azimuth coupling, and azimuth modulation. It is zero at the swath center because of the factor  $r$  in (29), but it exists at other ranges [6]. It is necessary to correct  $\Phi_V$  in a subsequent operation to focus precisely over the whole scene. In this paper, we prefer the Stolt interpolation (nonlinear mapping) to correct the nonlinear dependence of  $\Phi_V$  on the range and azimuth frequencies.
- 3)  $\Phi_{AS}(f_\tau)$  shows an intrinsic feature (i.e., azimuth scaling) of BiSAR in the azimuth-variant configuration, which can be removed with interpolation or ISFT.

Based on the aforementioned description, the range compression can also be incorporated into RFM. Thus, the RFM filter can be expressed as

$$H_{RFM}(f_\tau, f) = \exp[j\Phi_{IV}(f_\tau)] S_l^*(f) \exp\left\{-j2\pi \frac{R_m + p_{20}}{c} f\right\}. \quad (31)$$

The last exponential term of (31) denotes a phase correction to establish the phase reference to the scene center. The param-

eter  $p_{20}$  is the closest range from the scene center to the ideal trajectory of transmitter. After RFM filtering, the remaining bistatic signal is expressed as

$$\begin{aligned} G_1(f_\tau, f, r, \tau_{0R}) &= \bar{G}(f_\tau, f, R_{0R}, \tau_{0R}) \times H_{RFM} \\ &= \sigma(\tau_{0R}, R_{0R}) w(\tilde{\tau}_W - \tau_{cb}) \\ &\quad \times \exp\{-j[\Phi_V(f_\tau, f, r) + \Phi_{AS}(f_\tau)]\}. \end{aligned} \quad (32)$$

Based on (29), the Stolt interpolation can be expressed as [6], [17]

$$\frac{[cp_{11}k_T f_\tau + (F_{RW} + p_{21}F_{TW})]}{(1 + p_{21})} \rightarrow f_0 + f'. \quad (33)$$

This interpolation transformation is a nonlinear mapping of the original range-frequency variable  $f$  into a new range-frequency variable  $f'$  [6]. Substituting (33) into (29),  $\Phi_V$  can be rewritten as

$$\Phi_V(f_\tau, f, r) = 2\pi \frac{(1 + p_{21})r}{c} [f_0 + f']. \quad (34)$$

From (33), it can be seen that the range-variant RCM, range–azimuth coupling, and azimuth modulation are corrected by the nonlinear interpolation. A subsequent range FT will compress and register the signal in range

$$\begin{aligned} G_2(f_\tau, t, r, \tau_{0R}) &= \sigma(\tau_{0R}, R_{0R}) w(\tilde{\tau}_W - \tau_{cb}) \\ &\quad \times \exp[-j\Phi_{AS}(f_\tau)] p_r \left(t - \frac{(1 + p_{21})r}{c}\right) \end{aligned} \quad (35)$$

where  $p_r(t)$  is the compressed pulse envelope in the range. Because the azimuth dependence has been removed by the preprocessing step, we have  $R_{0R} + R_{0T} \approx R_m + p_{20} + (1 + p_{21})r$ . Thus, (35) can also be expressed as

$$\begin{aligned} G_2(f_\tau, t, r, \tau_{0R}) &= \sigma(\tau_{0R}, R_{0R}) w(\tilde{\tau}_W - s_{cb}) \\ &\quad \times \exp[-j\Phi_{AS}(f_\tau)] p_r \\ &\quad \times \left(t - \frac{R_{0R} - R_m + R_{0T} - p_{20}}{c}\right). \end{aligned} \quad (36)$$

Equation (36) implies that the range signal is registered to the relative position of scene center. At this stage, only an azimuth-scaling term remains. According to [4], an azimuth ISFT can be employed to correct the scaling and transform signal into the image domain.

$$\begin{aligned} G_3(t, R_m + r, \tau_{0R}) &= \sigma(\tau_{0R}, R_{0R}) p_r \left(t - \frac{(1 + p_{21})r}{c}\right) \\ &\quad \times \int w(\tilde{\tau}_W - \tau_{cb}) \exp[-j\Phi_{AS}(f_\tau)] \\ &\quad \times \exp(j2\pi \beta_A \tau f_\tau) d(\beta_A f_\tau) \\ &= \sigma(\tau_{0R}, R_{0R}) p_r \left(t - \frac{(1 + p_{21})r}{c}\right) \\ &\quad \times p_a(\tau - \tau_{0R}). \end{aligned} \quad (37)$$

In (37),  $p_a(\tau)$  is the compressed signal envelope in azimuth. Based on the aforementioned description, the processing steps of the proposed approach are shown in Fig. 2.

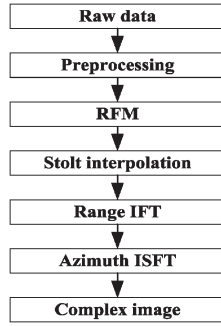


Fig. 2. Block diagram of WDA for BiSAR processing in spaceborne/airborne configurations.

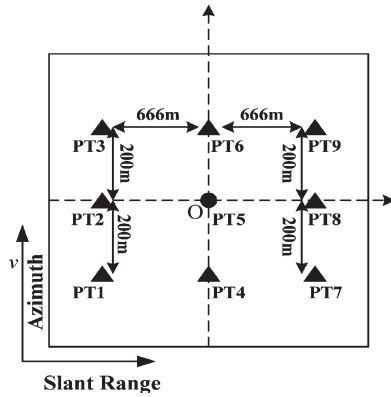


Fig. 3. Simulated scene with nine point targets.

#### IV. SIMULATION EXPERIMENT

In this section, we carry out some simulations, using the airborne SAR system parameters, FGAN's PAMIR, and satellite parameters of TerraSAR-X. This spaceborne/airborne hybrid experiment is being planned in cooperation with ZESS, FGAN/FHR, and DLR [15], [16], [18]. TerraSAR-X works in the sliding-spotlight mode; PAMIR is in the inverse sliding-spotlight mode, which is a special case of the sliding-spotlight mode [15], [18]. In this double sliding-spotlight model, azimuth spectrum's center frequency of a target depends on its azimuth coordinate, which implies that the azimuth scene has a higher bandwidth as compared to a single point target [18], [19]. Therefore, a higher pulse repetition frequency (PRF) is required to properly sample the azimuth signal.

The simulated scene consists of nine point targets, which are located on the vertices of a  $3 \times 3$  matrix, shown in Fig. 3.

The parameters are listed in Table I.

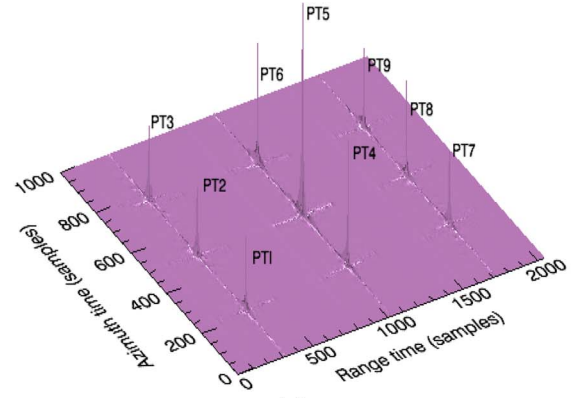
In this simulation, the maxima of the Doppler spectrum shift and Doppler bandwidth are  $-964$  and  $671$  Hz, respectively. Therefore, for the simulated scene, the excursion for azimuth frequency is less than  $1635$  Hz. Thus, a PRF of  $4000$  Hz can properly sample the simulated signal.

To emphasize the role of azimuth scaling, we first show the focusing result without the azimuth-scaling correction in Fig. 4(a).

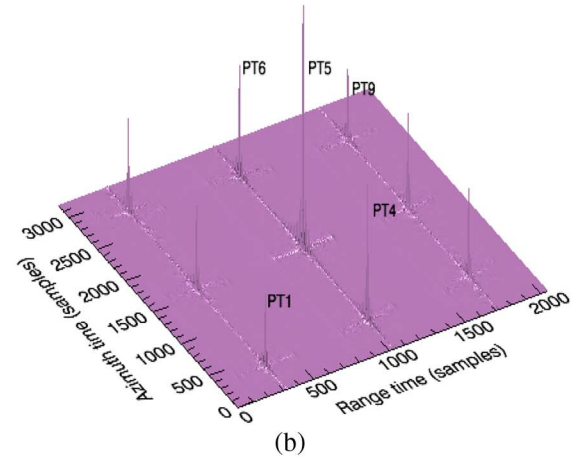
Before the azimuth-scaling correction, the azimuth relative distances of PT4 and PT6 to PT5 are  $6.375$  m (the theoretical distance is  $200$  m), i.e., the azimuth scene is compressed by a ratio of  $31.37$ , which implies that the scaling factor is  $0.031875$ . According to (31), the azimuth-scaling factor  $\beta_A$  is equal to

TABLE I  
SPACEBORNE/AIRBORNE SAR SYSTEM PARAMETERS

	PAMIR	TerraSAR-X
Carrier frequency	9.65 GHz	
bandwidth	150 MHz	
PRF	4000 Hz	
Velocity	100 m/s	7600 m/s
Altitude	3 km	514 km
Depression angle	$30^\circ$	$50^\circ$
Scan angle	$\pm 10.656^\circ$	$\pm 0.75^\circ$
Beam width	$2^\circ$	$0.33^\circ$
Sliding factor	8.9018	0.2851
Time-bandwidth product	2.89	149.26
Overlapping time of footprints	2.86 s	



(a)



(b)

Fig. 4. (a) Focused scene before azimuth-scaling correction. (b) Focused scene after azimuth-scaling correction.

$0.031901379$ . The error of the scaling correction is  $0.0827\%$ . Due to the limitation of computer's memory, we only correct the scaling to  $16.67\%$  of the real value and show it in Fig. 4(b).

Comparing Fig. 4(a) and (b), we can see that the azimuth scaling is considerably severe in this extreme azimuth-variant bistatic configuration.

To quantify the precision of the presented processing method, the impulse-response width (IRW), peak sidelobe ratio (PSLR), and integrated sidelobe ratio (ISLR) are used as quality criteria. A rectangular window is used in the range and azimuth processing.

To examine focusing quality in more detail, the target away from the center (i.e., PT9) is highlighted in more detail in Fig. 5.

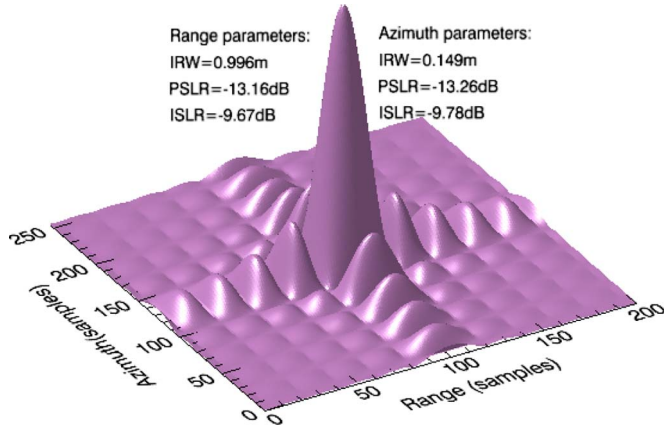


Fig. 5. Two-dimensional impulse response of PT9.

In Fig. 5, the azimuth PSLR and ISLR agree well with the theoretical values of  $-13.2$  and  $-9.7$  dB; the range PSLR and ISLR show a deviation of less than  $0.2$  dB with respect to the theoretical values; the measured range IRW and azimuth IRW agree nicely with the theoretical values of  $1$  and  $0.149$  m.

## V. CONCLUSION

In this paper, the original LBF is extended to focus the spaceborne/airborne hybrid BiSAR data. To facilitate processing, the QM term is linearized in both directions, which clearly shows the 2-D scaling phenomenon in the spaceborne/airborne hybrid bistatic configuration. We use Stolt interpolation to correct the range-variant range scaling (RCM), range-azimuth coupling, and azimuth modulation. In the spaceborne/airborne configuration, the additional azimuth scaling appears considerably severe. Moreover, it is corrected by using ISFT. The simulations validate the performance of the proposed model and method. The proposed signal mode and processing approach can also be applied to focus the BiSAR data in the azimuth-variant configurations. However, the range-azimuth partitioning is required in the preprocessing. More subsections mean expensive computational cost, but less subsections could result in an inaccurate compensation of the BD term.

## APPENDIX OVERVIEW OF WEIGHTING IDEA

This appendix shows how the weighting idea was developed. In the derivation of LBF, the same azimuth modulations of both of platforms are assumed. When both of platforms contribute unequally to the total azimuth modulation, this assumption would result in the inaccurate individual stationary points  $\tilde{\tau}_R$  and  $\tilde{\tau}_T$  [refer to (41)]. Accordingly, the inaccurate stationary points cannot represent the individual time-Doppler correspondences [20].<sup>1</sup> Therefore, the time differences  $(\tau - \tilde{\tau}_R)$  and  $(\tau - \tilde{\tau}_T)$  would become larger, which means that the neglected third or higher order phase terms in (11) as the functions of  $(\tau - \tilde{\tau}_R)$  and  $(\tau - \tilde{\tau}_T)$  would introduce a significant phase error and might further result in the failure of the second-order

<sup>1</sup>The instantaneous Doppler frequency  $f_\tau$  and the azimuth time variable  $\tau$  have an inverse relationship [20]. This relationship can be approximately represented by the stationary point  $\tilde{\tau}_p$ . When  $\tilde{\tau}_p$  accurately represent the time-Doppler correspondence, we approximately have  $\tilde{\tau}_p \approx \tau$ .

model which is the basis of deriving our bistatic spectrum [2]. The purpose of our weighting idea is to improve the accuracy of the quadratic mode around  $\tilde{\tau}_R$  and  $\tilde{\tau}_T$  by obtaining the more accurate individual time-Doppler correspondences. It can be implemented by making azimuth modulations of both range equations to agree with the individual instantaneous Doppler frequencies in the respective slant range histories.

The instantaneous Doppler frequency of the total range history in the spaceborne/airborne configuration (i.e., small squint case) can be formulated as [6]

$$f_\tau(\tau) = -\frac{f+f_0}{c} \frac{d}{d\tau} [R_R(\tau) + R_T(\tau)] \\ \approx \underbrace{-\frac{f+f_0}{c} \frac{v_R^2}{R_{0R}} (\tau - \tau_{cb})}_{\text{Receiver}} - \underbrace{\frac{f+f_0}{c} \frac{v_T^2}{R_{0T}} (\tau - \tau_{cb})}_{\text{Transmitter}}. \quad (38)$$

From (38), we see that the contributions of the Doppler modulations from the individual platform to the total instantaneous Doppler frequency are approximately proportional to the slopes of the respective range equations  $v_R^2/R_{0R}$  and  $v_T^2/R_{0T}$ . LBF works well when the ratio  $(v_R^2/R_{0R})/(v_T^2/R_{0T})$  is near unity. LBF would fail in cases where the ratio deviates from unity, e.g., in a spaceborne/airborne configuration.

Starting from (38), the weighted individual phase histories are formulated as in (9). To show validity of the weighting operation, we define the phase-error functions of the quadratic slant range histories of receiver and transmitter in (11) and [2] as

$$E_R(\tau, f) \approx \phi_R(\tau, f) - \left[ \phi_R(\tilde{\tau}_R, f) + \frac{1}{2} \ddot{\phi}_R(\tilde{\tau}_R, f) (\tau - \tilde{\tau}_R)^2 \right] \\ E_T(\tau, f) \approx \phi_T(\tau, f) - \left[ \phi_T(\tilde{\tau}_T, f) + \frac{1}{2} \ddot{\phi}_T(\tilde{\tau}_T, f) (\tau - \tilde{\tau}_T)^2 \right] \quad (39)$$

$$E_{RW}(\tau, f) = \phi_{RW}(\tau, f) - \left[ \phi_{RW}(\tilde{\tau}_{RW}, f) + \frac{1}{2} \ddot{\phi}_{RW}(\tilde{\tau}_{RW}, f) (\tau - \tilde{\tau}_{RW})^2 \right] \\ E_{TW}(\tau, f) = \phi_{TW}(\tau, f) - \left[ \phi_{TW}(\tilde{\tau}_{TW}, f) + \frac{1}{2} \ddot{\phi}_{TW}(\tilde{\tau}_{TW}, f) (\tau - \tilde{\tau}_{TW})^2 \right] \quad (40)$$

where  $\tilde{\tau}_R$  and  $\tilde{\tau}_T$  are defined as

$$\tilde{\tau}_R = \tau_{0R} - \frac{cR_{0R}}{2v_R^2} \frac{f_\tau}{F_R} \\ \tilde{\tau}_T = \tau_{0T} - \frac{cR_{0T}}{2v_T^2} \frac{f_\tau}{F_T} \quad (41)$$

$$F_R = \sqrt{(f+f_0)^2 - \left( \frac{cf_\tau}{2v_R} \right)^2} \\ F_T = \sqrt{(f+f_0)^2 - \left( \frac{cf_\tau}{2v_T} \right)^2}. \quad (42)$$

In this Appendix, PT9 is used as an example to display the approximation error of the quadratic model. The phase errors

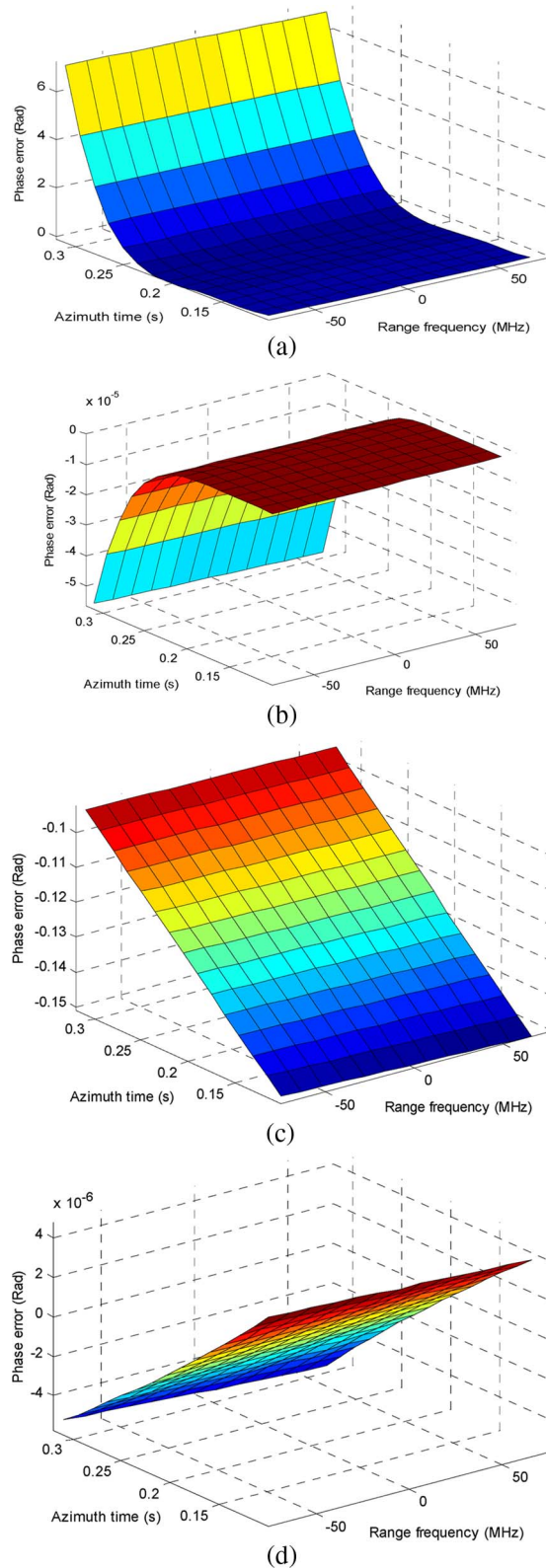


Fig. 6. (a)  $E_R(\tau, f)$ . (b)  $E_T(\tau, f)$ . (c)  $E_{RW}(\tau, f)$ . (d)  $E_{TW}(\tau, f)$ .

in the LBF ( $E_R$  and  $E_T$ ) are shown in Fig. 6(a) and (b); the phase errors for ELBF ( $E_{RW}$  and  $E_{TW}$ ) are shown in Fig. 6(c) and (d).

Fig. 6(a) shows that the phase error appears to be nonlinear in azimuth and approximately linear in range. It is the reason

why the focused point target in a spaceborne/airborne case by using the LBF deteriorates visibly in azimuth [5].

Comparing Fig. 6(a) and (b) with Fig. 6(c) and (d), it can be seen that the weighting operation can eliminate this phase error and results in a significant improvement of the accuracy of the quadratic mode in this spaceborne/airborne configuration.

In addition, the plots in Fig. 6(c) and (d) also shows that the larger the TBP of the slant range history is, the more accurate the second-order model will be. When the TBP is larger than 100, the slant range histories can be accurately represented by its second-order approximation [6], [20].

#### ACKNOWLEDGMENT

This paper reported herein is part of the joint German Science Foundation (DFG) research initiative Bistatic Exploration (PAK 59) of ZESS and FGAN, individually funded under Grant number "Lo 455/7-1," which is gratefully acknowledged. The authors would also like to point out the excellent and very effective cooperation between ZESS and FHR/FGAN, which is seen as a key item of their work. Finally, the authors would like to thank the anonymous reviewers for their very constructive and encouraging comments, helping to improve this paper.

#### REFERENCES

- [1] J. H. Ender, I. Walterscheid, and A. Brenner, "New aspects of bistatic SAR: Processing and experiments," in *Proc. IGARSS*, Anchorage, AK, Sep. 2004, pp. 1758–1762.
- [2] O. Loffeld, H. Nies, V. Peters, and S. Knedlik, "Models and useful relations for bistatic SAR processing," *IEEE Trans. Geosci. Remote Sens.*, vol. 42, no. 10, pp. 2031–2038, Oct. 2004.
- [3] O. Arikan and D. C. Munson, Jr., "A tomographic formulation of bistatic synthetic aperture radar," in *Proc. Comcon*, Baton Rouge, LA, Oct. 1988, p. 418.
- [4] K. Natroshvili, O. Loffeld, H. Nies, A. Medrano-Ortiz, and S. Knedlik, "Focusing of general bistatic SAR configuration data with 2-D inverse scaled FFT," *IEEE Trans. Geosci. Remote Sens.*, vol. 44, no. 10, pp. 2718–2727, Oct. 2006.
- [5] R. Wang, O. Loffeld, H. Qurat Ul-Ann, A. Nies, and A. Medrano-Ortiz, "A bistatic point target reference spectrum for general bistatic SAR processing," *IEEE Geosci. Remote Sens. Lett.*, vol. 5, no. 3, pp. 517–521, Jul. 2008.
- [6] I. G. Cumming and F. H. Wong, *Digital Processing of Synthetic Aperture Radar Data Algorithms and Implementation*. Norwood, MA: Artech House, 2005.
- [7] I. Walterscheid, J. H. G. Ender, A. R. Brenner, and O. Loffeld, "Bistatic SAR processing and experiments," *IEEE Trans. Geosci. Remote Sens.*, vol. 44, no. 10, pp. 2710–2717, Oct. 2006.
- [8] R. Bamler, F. Meyer, and W. Liebhart, "Processing of bistatic SAR data from quasi-stationary configurations," *IEEE Trans. Geosci. Remote Sens.*, vol. 45, no. 11, pp. 3350–3358, Nov. 2007.
- [9] D. D'Aria, A. M. Guarnieri, and F. Rocca, "Focusing bistatic synthetic aperture radar using dip move out," *IEEE Trans. Geosci. Remote Sens.*, vol. 42, no. 7, pp. 1362–1376, Jul. 2004.
- [10] M. Antoniou, R. Saini, and M. Cherniakov, "Results of a space–surface bistatic SAR image formation algorithm," *IEEE Trans. Geosci. Remote Sens.*, vol. 45, no. 11, pp. 3359–3371, Nov. 2007.
- [11] Y. L. Neo, F. H. Wong, and I. G. Cumming, "A two-dimensional spectrum for bistatic SAR processing using series reversion," *IEEE Geosci. Remote Sens. Lett.*, vol. 4, no. 1, pp. 93–96, Jan. 2007.
- [12] F. H. Wong, I. G. Cumming, and Y. L. Neo, "Focusing bistatic SAR data using nonlinear chirp scaling algorithm," *IEEE Trans. Geosci. Remote Sens.*, vol. 46, no. 9, pp. 2493–2505, Sep. 2008.
- [13] Y. L. Neo, F. Wong, and I. G. Cumming, "Processing of azimuth-invariant bistatic SAR data using the range Doppler algorithm," *IEEE Trans. Geosci. Remote Sens.*, vol. 46, no. 1, pp. 14–21, Jan. 2008.
- [14] R. Wang, O. Loffeld, Q. Ul-Ann, H. Nies, A. Medrano-Ortiz, and S. Knedlik, "Analysis and extension of Loffeld's bistatic formula in

spaceborne/airborne configuration,” in *Proc. EUSAR*, Friedrichshafen, Germany, Jun. 2008. CD-ROM.

- [15] J. H. G. Ender, “The double sliding spotlight mode for bistatic SAR,” in *Proc. IRS*, Cologne, Germany, Sep. 2007, pp. 329–333.
- [16] I. Walterscheid, T. Espeter, and J. H. G. Ender, “Performance analysis of a hybrid bistatic SAR system operating in the double sliding spotlight mode,” in *Proc. IGARSS*, Barcelona, Spain, Jul. 2007, pp. 2144–2147.
- [17] R. H. Stolt, “Migration by transform,” *Geophysics*, vol. 43, no. 1, pp. 23–48, Feb. 1978.
- [18] R. Wang, O. Loffeld, H. Nies, S. Knedlik, Q. Ul-Ann, A. Medrano-Ortiz, and J. H. G. Ender, “Frequency-domain bistatic SAR processing for spaceborne/airborne configuration,” *IEEE Trans. Aerosp. Electron. Syst.*, to be published.
- [19] D. P. Belcherand and C. J. Baker, “High resolution processing of hybrid strip-map/spotlight mode SAR,” *Proc. Inst. Elect. Eng.—Radar, Sonar, Navig.*, vol. 143, no. 6, pp. 366–374, Dec. 1996.
- [20] C. E. Cook and M. Bernfeld, *Radar Signal: An Introduction to Theory and Application*. New York: Academic, 1967.



raw-signal simulation.

**Robert Wang** (M’07) received the B.S. degree in control engineering from the University of Henan, Kaifeng, China, in 2002 and the Dr. Eng. degree from the Graduate University of the Chinese Academy of Sciences, Beijing, China, in 2007.

Since 2007, he has been with the Center for Sensorsystems, University of Siegen, Siegen, Germany. He is currently working on the hybrid bistatic experiment. His research interests include monostatic and bistatic SAR signal processing, bistatic interferometric airborne SAR motion compensation, and SAR

**Otmar Loffeld** (M’05–SM’06) received the Diploma degree in electrical engineering from the Technical University of Aachen, Aachen, Germany, in 1982 and the Eng. Dr. degree and the “Habilitation” in the field of digital signal processing and estimation theory from the University of Siegen, Siegen, Germany, in 1986 and 1989, respectively.

Since 1991, he has been a Professor for digital signal processing and estimation theory with the University of Siegen, where he has been giving lectures on general communication theory, digital signal processing, stochastic models and estimation theory, and synthetic aperture radar. He is the author of two textbooks on estimation theory. Since 1995, he has been a member of the Center for Sensorsystems (ZESS) which is a central scientific research establishment at the University of Siegen, where since 2005, he has been the Chairman. In 1999, he was a Principal Investigator (PI) on baseline estimation for the X-band part of the Shuttle Radar Topography Mission, where ZESS contributed to DLR’s baseline-calibration algorithms. In 2002, he founded the International Postgraduate Program “Multi Sensorics,” and, based on that program, he established the “NRW Research School on Multi Modal Sensor Systems for Environmental Exploration and Safety (MOSES)” at the University of Siegen as an upgrade of excellence in 2008. He is the Speaker and Coordinator of both doctoral degree programs hosted by ZESS. He is also the Scientific Coordinator for “Multidimensional and Imaging Systems” at the University of Siegen. He is a PI for interferometric techniques in the German TerraSAR-X mission, and together with Prof. Ender from Forschungsgesellschaft für Angewandte Naturwissenschaften (FGAN), is one of the PIs for a bistatic spaceborne–airborne experiment, where TerraSAR-X serves as the bistatic illuminator while FGAN’s PAMIR system mounted on a Transall airplane is used as a bistatic receiver. His current research interests include multisensor data fusion, Kalman filtering techniques for data fusion, optimal filtering and process identification, SAR processing and simulation, SAR interferometry, phase unwrapping, and baseline estimation. A recent field of interest is bistatic SAR processing.

Dr. Loffeld is a member of the ITG/VDE and a member of the IEEE Geoscience and Remote Sensing Society. He was the recipient of the Scientific Research Award of North Rhine-Westphalia (“Bennigsen-Foerder Preis”) for his works on applying Kalman filters to phase-estimation problems such as Doppler centroid estimation in SAR, phase, and frequency demodulation.



**Holger Nies** received the Diploma degree in electrical engineering and the Dr. Eng. degree from the University of Siegen, Siegen, Germany, in 1999 and 2006, respectively.

Since 1999, he has been a member of the Center for Sensorsystems (ZESS), University of Siegen, where he has been working in the project sector “Optimal Signal Processing, Remote Sensing—SAR” and has also been a Lecturer with the Department of Signal Processing and Communication Theory. He was also involved in some project work for Daimler AG, Stuttgart, Germany, in the field of engine modeling and optimization. He is currently working in the area of interferometric techniques in the German TerraSAR-X mission. His research interests include bistatic SAR processing, SAR interferometry, and distributed data fusion.

Dr. Nies was the recipient of the Best Poster Award at the Sixth European Conference on Synthetic Aperture Radar, Dresden, Germany, in 2006.



**Joachim H. G. Ender** (M’02–SM’06) received the Diploma degree in mathematics and physics from the Westphalian Wilhelm University of Münster, Münster, Germany, in 1975 and the Ph.D. degree in electrical engineering from Ruhr-University Bochum, Bochum, Germany.

In 1976, he was with the Research Establishment of Applied Science (Forschungsgesellschaft für Angewandte Naturwissenschaften, FGAN), Wachtberg, Germany. Since 1992, he has been giving annual lectures on radar signal processing

with Ruhr-University Bochum, which conferred the title Honorary Professor upon him in 2002. He also gives lectures on radar techniques at the Rhineish-Westphalian Technical University, Aachen, Germany, and the University of Siegen, Siegen, Germany. In 1999, he was the Head of the Electronics Department, Research Institute for High Frequency Physics and Radar Techniques (FHR), FGAN, where he initiated and supervised research activities for various aspects of phased array and imaging radars, including the design and operation of experimental SAR systems, such as AER-II and PAMIR, and where since 2003, he has been the Director of FHR, and in August 2007, was elected Vice Chairman of FGAN. He is an Executive Board Member of the German Institute of Navigation, as well as Member-at-Large of the North Atlantic Treaty Organization Sensors and Electronics Technology Research Panel. He further acts as Review Board Member of the German Research Foundation and as a Review Board Member of the Leibniz Society. He has authored and coauthored numerous papers in various international journals and conferences. His current research interests include very high resolution SAR imaging, 3-D SAR, MIMO SAR, multibaseline and wideband processing techniques for across-track SAR interferometry, ground moving-target indication with air- and space-based radar including multistatic satellite constellations, inverse SAR for moving-target imaging, and bistatic SAR processing.

Dr. Ender, jointly with colleagues, was the recipient of the German Society for Information Technology Paper Prize Award of the Association of German Electrical Engineers in 1992 and the IEEE TRANSACTIONS ON GEOSCIENCE AND REMOTE SENSING Best Paper Award in 2006. In 1996, he was one of the founding members of the biannual “European Conference on Synthetic Aperture Radar.”